LANGMUIR

pubs.acs.org/Langmuir Article

Systematic Quantification of Electron Transfer in a Bare Phospholipid Membrane Using Nitroxide-Labeled Stearic Acids: Distance Dependence, Kinetics, and Activation Parameters

Max Schmallegger, Antonio Barbon,* Marco Bortolus, Angela Chemelli, Itzhak Bilkis, Georg Gescheidt,* and Lev Weiner*

Cite This: https://dx.doi.org/10.1021/acs.langmuir.0c01585 Read Online

ACCESS | Metrics & More | Article Recommendations | Supporting Information

ABSTRACT: In this report, we present a method to characterize the kinetics of electron transfer across the bilayer of a unilamellar liposome composed of 1,2-dimyristoyl-*sn*-glycero-3-phosphocholine. The method utilizes synthetic phospholipids containing noninvasive nitroxide spin labels having the >N−O• moiety at well-defined distances from the outer surface of the liposome to serve as reporters for their local environment and, at the same time, permit measurement of the kinetics of electron transfer. We used 5-doxyl and 16-doxyl stearic acids. The paramagnetic >N−O• moiety is photo-oxidized to the corresponding diamagnetic oxoammonium cation by a ruthenium electron acceptor formed in the solution. Electron transfer is monitored by three independent spectroscopic methods: by both steady-state and time-resolved electron paramagnetic resonance and by optical spectroscopy. These techniques allowed us to differentiate between the electron transfer rates of nitroxides located in the outer leaflet of the phospholipid bilayer and of those located in the inner leaflet. Measurement of electron transfer rates as a function of temperature revealed a low-activation barrier ($\Delta G^{\ddagger} \sim 40$ kJ/mol) that supports a tunneling mechanism.

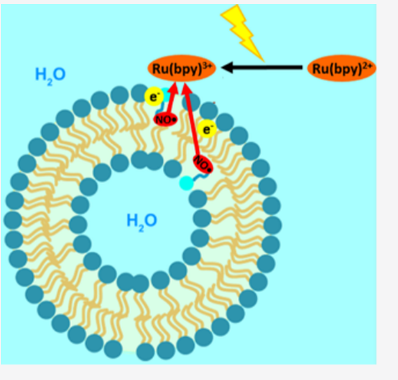

■ INTRODUCTION

Electron transfer (ET) is one of the principal processes involved in harvesting and transferring energy in natural and artificial systems. Indeed, it is an essential process in all living organisms.[1−3] Extensive studies of ET have been performed on proteins,[1,4,5] DNA,[6,7] dendrimers,[8] and artificial photosynthetic centers.[9,10] A consistent effort is devoted to the ET across lipid membranes.[11] Most of studies on ET across biological membranes focus on natural or artificial redox-active complexes embedded in a lipid bilayer and on the effects of the presence of cations, on the processes of electron and proton transfer.[12,13] The study of membranes is relevant to solar energy conversion.[12,14−19] Also, knowledge of ET across membranes is fundamental both for understanding the functioning of natural photosynthetic systems and for creating their artificial analogs.[12,20] The contribution of the fatty-acid chains of the phospholipids to ET is poorly understood. The roles of the main types of chemical bonds, that is, hydrogen-, π-, and σ-bonds in ET are not well understood either.[13,21,22]

In studies on membrane systems, unilamellar liposomes are often used as model systems,[23−27] with the donor and acceptor being separated by a lipid bilayer. In general, methods that rely on optical spectroscopies utilize bulky and rigid dyes, inferring perturbations to the system; it is a challenge to identify probes that do not substantially alter the membrane, and, at the same time, provide clear-cut information on the ET phenomena.[12,14,17,19,23−26,28−30] Another challenge for the methods is the flexibility to cover kinetics extending over several orders of magnitude.

Electron paramagnetic resonance (EPR) spectroscopy represents an interesting option for studying reaction kinetics in a wide range of time scales, from microseconds[31] to hours.[32] It requires a paramagnetic center in the system, but, with respect to popular optical spectroscopies, it overcomes the disadvantage of coping with unresolved and overlapping optical absorptions or background signals.

Here, we present a novel and highly efficient methodology for studying ET across membranes based on EPR. We make use of nitroxides as paramagnetic centers that are attached to stearic acids in different positions to localize them at different depths in the membrane. These molecules have been selected as they do not substantially perturb the phospholipid bilayer.[33−36] Photoinduced oxidation of the nitroxides, using a well-established procedure, yields time-dependent EPR signal intensities that can be straightforwardly translated into kinetic data. It is a key advantage that the study of the EPR spectra

Received: May 28, 2020
Revised: July 24, 2020
Published: July 26, 2020

(eventually in the presence of added relaxants) can provide relevant information both on the positioning of the nitroxide moiety within the bilayer; and on the environment of the probe.

Use of these probes enables us to systematically address the contribution of the phospholipids to ET across a biological membrane. It is important to distinguish this "background" contribution if one wants to focus on ET of active constituents, such as proteins and metal complexes dissolved into the membrane.

Two probes, 5-doxyl stearic acid (**5DSA**) and 16-doxyl stearic acid (**16DSA**) (Scheme 1), were introduced into unilamellar liposomes composed of 1,2 dimyristoyl-*sn*-glycero-3-phosphocholine (DMPC).[37,38] While in **5DSA** the nitroxide moiety is located adjacent to the hydrophilic moiety of DMPC, in **16DSA** it resides deep within the lipophilic domain.[39] Molecular dynamics simulations predicted **5DSA** to be located only ~ 0.5 nm from the membrane surface. For **16DSA** the distance increases to ~ 1.8 nm.[39] These distinctly differing locations of the probes are, therefore, well suited to obtaining insight into the distance dependence of the ET process.

Scheme 1. Phospholipid 1,2-Dimyristoyl-*sn*-glycero-3-phosphocholine (DMPC) and Stable Nitroxide Radicals (SNRs) 5DSA and 16DSA

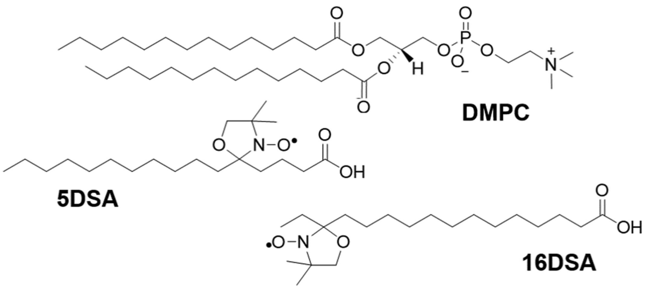

We selected DMPC-based membranes since they display a transition from a gel-like to a liquid crystalline phase at room temperature (296.6 K).[40] This allows us to investigate the influence of the rigidity of the lipid bilayer on ET. In the liquid crystalline state, lateral diffusion of lipids within the vesicle bilayer is rapid, whereas the transverse "flip-flop" motion is extremely slow.[41] Below 296.6 K, the transition to the gel-like phase causes all modes of mobility to decrease by orders of magnitude.[42,43]

To monitor the ET kinetics, we needed a reaction sequence that could be triggered. Here, we utilized the well-established photoinduced oxidation of $[Ru(bpy)_3]^{2+}$ to $[Ru(bpy)_3]^{3+}$ in the presence of ammonium persulfate ($(NH_4)_2S_2O_8$).[44−50] The decisive and rate-limiting step is the subsequent oxidation of the nitroxide moiety by ground-state $[Ru(bpy)_3]^{3+}$. The reaction produces the EPR-silent oxoammonium cation (OAC), with concomitant regeneration of $[Ru(bpy)_3]^{2+}$ (Scheme 2). This approach has been used successfully for monitoring ET reactions,[31,44,51] since the photoinduced formation of $[Ru(bpy)_3]^{3+}$ is faster than its reaction with $RNO^\bullet$; furthermore, the Ru-complex is highly water-soluble, therefore it does not diffuse into the membrane.

The complex $[Ru(bpy)_3]^{2+}$ displays strong absorption at 452 nm. Following the decrease in absorption at this wavelength thus provides an additional tool for following the ET kinetics.[46,52,53]

Scheme 2. Photoinduced Oxidation of a Nitroxide to the Corresponding Oxoammonium Cation by Photoexcitation of $[Ru(bpy)_3]^{2+}$ to its Excited State $[Ru(bpy)_3]^{2+*}$ via a Metal-to-Ligand Charge Transfer ($k_{exc} \geq 5 \times 10^{10}$ s^{-1})[54] Followed by Oxidation of $[Ru(bpy)_3]^{2+*}$ to $[Ru(bpy)_3]^{3+}$ in the Presence of $(NH_4)_2S_2O_8$

$$[Ru(bpy)_3]^{2+} \xrightarrow{h\nu,\, k_{exc}} [Ru(bpy)_3]^{2+*}$$

$$2\,[Ru(bpy)_3]^{2+*} + S_2O_8^{2-} \xrightarrow{k_{ox}} 2\,[Ru(bpy)_3]^{3+} + 2\,SO_4^{2-}$$

$$[Ru(bpy)_3]^{3+} + RNO\bullet \xrightarrow{k_{NO\bullet}} [Ru(bpy)_3]^{2+} + RNO^{+}$$

To obtain a strong set of experimental data, we followed the kinetics of the reactions displayed in Scheme 2 by steady-state EPR (continuous irradiation), by laser-triggered time-resolved EPR, and by optical absorption spectroscopy.

EXPERIMENTAL SECTION

Liposome Preparation. Liposomes were prepared by ultrasonication.[54] Briefly, the phospholipid and the corresponding stable nitroxide radical (SNR) (w/w 50:1) were dissolved in 0.5 mL dichloromethane and dried to a thin film under a nitrogen stream in a test tube at room temperature. After further drying for 1 h under vacuum, the film was hydrated with 1 mL of buffer at neutral pH and then sonicated for 15 min. Residual free SNRs were removed by dialysis, and their complete removal checked by EPR.

Liposome Characterization by Small-Angle X-ray Scattering (SAXS). The measurements utilized a SAXSpoint 2.0 (Anton Paar, Graz, Austria) apparatus containing a Primux 100 micro microfocus X-ray source operating at λ = 0.154 nm (Cu-K$_\alpha$). Two-dimensional scattering patterns were recorded by a 2D EIGER R Series Hybrid Photon Counting (HPC) detector (Dectris Ltd., Baden-Daettwil, Switzerland). The samples were inserted into a capillary (1 mm diameter) and measured nine times for 300 s. The scattering patterns were averaged and compensated for the cosmic X-ray impacts. All measurements were performed at 20 °C. Absolute scale calibration was achieved by using water as a secondary standard.[55] All SAXS data were evaluated by a generalized indirect Fourier transform (GIFT) method to determine the pair distance distribution functions.[56−58]

Liposome Characterization by Dynamic Light Scattering. The dynamic light scattering (DLS) equipment consisted of a diode laser (Coherent Verdi V5, λ = 532 nm) and a goniometer with single-mode fiber detection optics (OZ from GMP, Zürich, Switzerland). The data were acquired by an ALV/SO-SIPD/DUAL photomultiplier with pseudocross correlation and an ALV 7004 Digital Multiple Tau Real Time Correlator (ALV, Langen, Germany). The ALV software package was used to record and store the correlation functions. Light scattering was measured five times for 30 s, at a scattering angle of 90° and a temperature of 25 °C, and the resulting correlation functions were averaged. The hydrodynamic radius was calculated using optimized regulation technique software.[59]

Continuous-Wave Electron Paramagnetic Resonance. Continuous wave (cw) EPR spectra were recorded on a Bruker X-band spectrometer (EMX, 100 kHz field modulation) at 275, 283, 303, and 310 K with a 0.15 mT field modulation amplitude. Photolysis was conducted using a Hamamatsu Lightingcure LC4 Xe/Hg lamp. The correlation times were calculated using the MATLAB-based GUI SimLabel.[60] The concentration of the SNR was 2×10^{-5} M in all measurements. The concentration of $[Ru(bpy)_3]Cl_2$ and $(NH_4)_2S_2O_8$ were 1×10^{-5} and 5×10^{-4} M, respectively.

Power Saturation Experiments. The power saturation experiments for determining the position of the nitroxide moieties within the bilayer of the DMPC liposomes were performed on an E580 ELEXSYS Bruker X-band spectrometer, equipped with a room-temperature dielectric resonator, ER4123D. All spectra were obtained using the following parameters: modulation amplitude 0.15 mT; modulation frequency 100 kHz; time constant 82 ms; conversion time

https://dx.doi.org/10.1021/acs.langmuir.0c01585
Langmuir XXXX, XXX, XXX−XXX

Scheme 3. Kinetic Equations and Boundary Conditions Used for the Simulation of the Time-Dependent Decrease of the EPR signal of 5DSA and 16DSA Nitroxides and Graphical Representation of the Inner and outer ET Pathways[a]

$$[Ru(bpy)_3]^{3+} \begin{cases} + RNO^{\bullet}_{outer} \xrightleftharpoons{k_{outer}} [Ru(bpy)_3]^{2+} + RNO^{+}_{outer} & (1) \\ + RNO^{\bullet}_{inner} \xrightleftharpoons{k_{inner}} [Ru(bpy)_3]^{2+} + RNO^{+}_{inner} & (2) \end{cases}$$

$$c(RNO^{\bullet}_{total}) = c(RNO^{\bullet}_{inner}) + c(RNO^{\bullet}_{outer}) \quad (3)$$

$$c(RNO^{\bullet}_{inner}) = c(RNO^{\bullet}_{outer}) \quad (4)$$

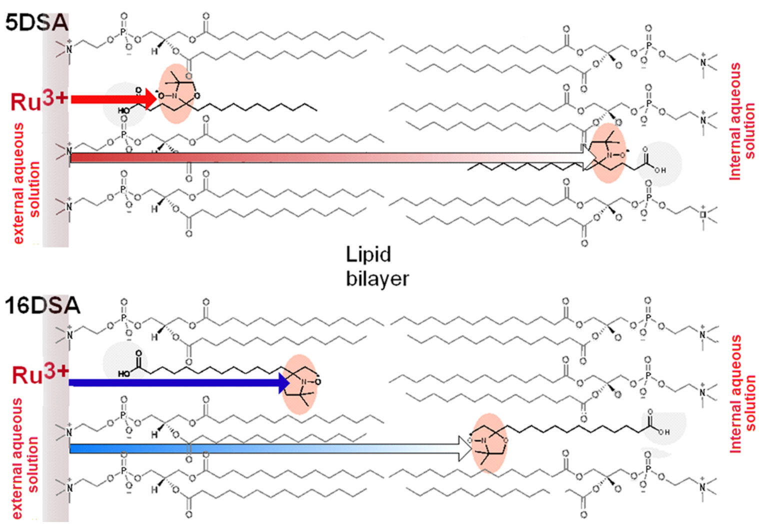

[a] $[Ru(bpy)_3]^{3+}$ is formed according to Scheme 2 in a rather short time scale ($k_{ox} = 1.2 \times 10^9$ M^{-1} s^{-1}).[48] It is reduced to $[Ru(bpy)_3]^{2+}$ by the nitroxide groups (oxidized to OAC) in a bimolecular process acting as the bottleneck of the ET process, eqs (1) and (2), and eqs (3) and (4) represent kinetic boundary conditions

164 ms; scan width 1.5 mT; 512 points; and temperature 293 K. The microwave power was ramped up automatically from 0.05 to 127 mW. The experimental protocol for the insertion depth measurements was as follows: approximately 5 μL samples were loaded into a gas permeable TPX capillary (L&M EPR Supplies, Inc., Milwaukee, WI, USA), and three saturation experiments were performed. The first experiment was done on the sample in equilibrium with air, to saturate the membrane with oxygen. The second experiment was performed on the same sample after deoxygenation under dry nitrogen flow for 20 min. The third experiment was carried out on a new sample to which a nickel complex with ethylenediaminediacetic acid (NiEDDA) had been added to a final concentration of 20 mM; the sample was then deoxygenated as mentioned above. The three power saturation curves (intensity vs microwave power) were obtained using a home-written program in Matlab that extracts the peak-to-peak amplitudes of the central line of the EPR spectra of the above experiments. The saturation curves were fitted using the standard equation:[27,61,62]

$$y = A\cdot\frac{x^{1/2}}{\left[1 + (2^{1/h} - 1)\cdot\frac{x}{p_{1/2}}\right]^{h}} \quad (1)$$

where $p_{1/2}$ is the saturation parameter, namely, the power at which the first derivative amplitude is reduced to half of its unsaturated value, h is the homogeneity parameter, indicating the homogeneity of saturation of the resonance line (ranging from h = 1.5 for a fully homogeneous line to h = 0.5 for a fully inhomogeneous line), and A is a scaling factor that accounts for the absolute signal intensity. The dimensionless parameter (Φ) that is related to the immersion depth of the nitroxide inside the membrane can be directly calculated from the ratio of the $p_{1/2}$ parameters obtained from the fitting of the data from the three experiments described above:

$$\Phi = \ln\frac{p_{1/2}^{oxygen} - p_{1/2}^{nitrogen}}{p_{1/2}^{NiEDDA} - p_{1/2}^{nitrogen}} \quad (2)$$

Time-Resolved Electron Paramagnetic Resonance. Time-resolved EPR (TR-EPR) signals were collected using the instrument lock-in amplifier connected to a fast digitizer on an E580 ELEXSYS Bruker X-band spectrometer. The modulation frequency was 100 kHz, and the modulation amplitude was 0.2 mT. The modulation of the magnetic field was set to a frequency of 100 kHz so that the time resolution was regulated by the time constant value (TC) to a maximum value of ∼ 10 μs. The experimental procedure involved a single laser pulse to photoexcite $[Ru(bpy)_3Cl_2]$, thus initiating the ET process as depicted in Scheme 2 followed by monitoring the decay of the EPR signal. Photoexcitation was performed using a Quantel Rainbow Nd:YAG laser (1064 nm) mounted with second and third harmonic modules and an optical parameteric oscillator. The final irradiation wavelength was set to 436 nm. The concentration of the SNR was 6.4×10^{-4} M in all measurements.

Time-Resolved UV–visible Spectroscopy. TR-UV-vis spectra were recorded on a UV-vis spectrometer equipped with optical fibers and a 1024-pixel diode-array detector (J&M Analytik AG, Essingen, Germany). Standard fluorescence quartz cuvettes were used for all measurements. Excitation of the samples was performed using a Hamamatsu Lightingcure LC4 Xe/Hg lamp. The concentration of the

https://dx.doi.org/10.1021/acs.langmuir.0c01585
Langmuir XXXX, XXX, XXX−XXX

SNR was 1×10^{-5} M for all measurements. The concentrations of $[Ru(bpy)_3]Cl_2$ and $(NH_4)_2S_2O_8$ were 1.41×10^{-5} and 5×10^{-4} M, respectively, for all measurements. The cuvette was irradiated for 30 s before each measurement, so as to convert all the $[Ru(bpy)_3]^{2+}$ to its oxidized form. After injection of the liposomes containing the SNRs, the absorbance at 452 nm was monitored with readings acquired at 1 s intervals.

Kinetic Analysis. Kinetic analysis was conducted using the kinetic reaction shown in Scheme 3 and explained in greater detail in the Supporting Information. The rate constants from the literature data were used where possible (Supporting Information, Schemes S1 and S2). The rate constants for the other reactions were determined by fitting the experimental curves with COPASI, a free software.[63] Two second-order distance-dependent reactions were used for the limiting-step electron transfer reaction for both **5DSA** and **16DSA**.

■ RESULTS AND DISCUSSION

Structure of the Liposomes and Properties of the Spin Probes. It was first necessary to establish that the presence of the spin-labeled fatty acids does not affect the integrity of the membrane. DLS measurements reveal that both the unmodified liposomes and those containing either **5DSA** or **16DSA** have a narrow size distribution, with an average hydrodynamic radius of 53 nm (see Supporting Information, Figure S5). SAXS shows that the thicknesses of the liposomes (ca. 5.1 nm, a result corroborated by molecular dynamics simulations),[62] is insignificantly altered when either of the probes resides in the membrane (see Supporting Information, Figure S4). We conclude that insertion of the phospholipids containing the SNRs does not significantly perturb the membrane structure.

Besides being a pivotal reactant in the ET reaction, the $RNO^\bullet$ group also serves as an efficient probe of the local environment. Figure 1 shows the temperature-dependent EPR spectra of **16DSA** and **5DSA**. Significantly, the signals detected for **16DSA** display narrower spectral lines than those of **5DSA**.

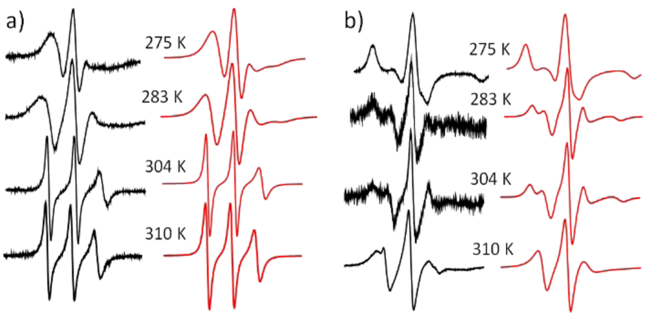

Figure 1. Temperature-dependent cw-EPR spectra of (a) **16DSA,** and (b) **5DSA** embedded in **DMPC** liposomes in aqueous solution (experimental, black; simulations, red). The data are shown in Table S1. Note that the experimental spectra do not contain components corresponding to spin labels in the aqueous phase outside the lipid bilayer.

This is a direct indication that the $NO^\bullet$ group of the **16DSA** resides in an environment whose density/viscosity is substantially lower than that of the surrounding **5DSA**. Above the transition temperature, in the liquid-crystal phase (>296.6 K), for both probes the lines become narrower, revealing higher mobility (much shorter rotational correlation times, see Supporting Information Table S1). These temperature-dependent lineshape changes are reversible. The data obtained are in line with **16DSA** being positioned in the rather flexible, lipophilic environment toward the center of the bilayer, while **5DSA** resides in a more ordered, rigid, and hydrophilic region close to the polar head group.[38,64−67] Our experimental data correspond well with the MD simulations referred to in the introduction.[39] Simulations evidence that all the EPR signals measured represent single species. This demonstrates that each label occupies a well-defined position within the membrane (on the EPR time scale) and confirms that no labels are detectable in the aqueous solution outside the membrane.

It has been reported that the fatty-acid-based chains bearing the labels may fold back within the bilayer.[36] Such a process would substantially affect the evaluation of the distance dependence. We, therefore, used power saturation EPR to experimentally address this issue. This method provides the depth parameter Φ (see the Experimental Section, and also Supporting Information Figure S8 and Table S2), which is a measure of the immersion depth of the spin label.[61] Φ values of 1.5 and 2.9 were obtained for **5DSA** and **16DSA**, respectively. These values are very similar to those reported for structurally related **5DPC** (1-palmitoyl-2-stearoyl-(5-doxyl)-sn-glycero-3-phosphocholine, Φ = 1.4) and **14DPC** (1-palmitoyl-2-stearoyl-(14-doxyl)-sn-glycero-3-phosphocholine, Φ = 3.0) in comparable POPC membranes (Table S2).[68] This strengthens our contention that the nitroxide moiety in **16DSA** is positioned substantially deeper within the bilayer than **5DSA**, and that back-folding does not make a substantial contribution, in agreement with earlier findings.[69]

Kinetics. After preparing and characterizing the unilamellar phospholipid vesicles and their nitroxide-labeled derivatives, they were added to a solution containing $[Ru(bpy)_3Cl_2]$ and $(NH_4)_2S_2O_8$. As shown in Scheme 2, irradiation converts the Ru(II) complex (present in the external aqueous phase) to Ru(III), which then oxidizes the paramagnetic nitroxide moiety to the EPR-silent oxoammonium cation. Accordingly, the Ru complex in the outer aqueous phase can interact with the nitroxide residing in the adjacent outer leaflet and a more distant one in the inner leaflet. This has to be accounted for in the kinetic equations, which are represented in Scheme 3. Consequently, the oxidation of the nitroxide moiety has to be split into two components: one accounting for the shorter (k_{outer}) and one for the longer (k_{inner}) distance. In terms of the overall concentration of the spin labels, we assume that they are evenly distributed between the inner and outer leaflet (eqs 3 and 4 in Scheme 3). The overall reaction scheme is therefore the combination of Schemes 2, and 3, and it is shown in Schemes S1 and S2 (See the Supporting Information) for the two cases of symmetric and nonsymmetric liposomes. The numerical solution of the overall equation scheme as described in the Experimental Section allows the determination of the concentration of all species and the fitting of all the experimental traces.

EPR time traces obtained under steady-state irradiation of nonsymmetrically prepared liposomes are displayed in Figure 2a−d. These curves reveal two reaction regimes, one dominating at short times, the second emerging after about 10 s. This is consistent with the presence of reactions 1 and 2 in Scheme 3, since ruthenium resides only in the solution outside the liposome (see Scheme S1). Our hypothesis has been verified using symmetric liposomes (Figure 2e−h, see below). The presence of two distinct rates for the two leaflets is possible since the nitroxides do not quickly exchange between the two leaflets in the time frame of the experiments,

https://dx.doi.org/10.1021/acs.langmuir.0c01585
Langmuir XXXX, XXX, XXX−XXX

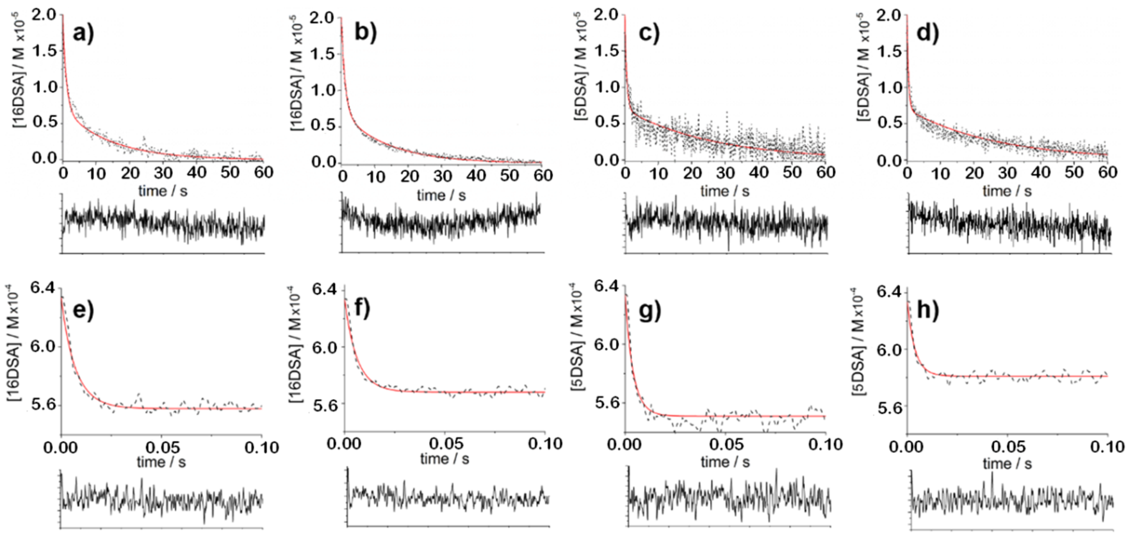

Figure 2. EPR intensity vs time detected upon steady-state irradiation (Black, experimental; red, simulated; and the residuals are shown below the decay curves). For the reactions, see Scheme 2. (a) **16DSA** at 283 K, (b) **16DSA** at 304 K, (c) **5DSA** at 283 K, and (d) **5DSA** at 304 K. In these experiments, the photoredox system is located only in the aqueous phase outside the liposome. Analogous curves are obtained upon pulsed-laser irradiation, (e−h). Here, the photoredox system is present in the external and in the internal aqueous phase. Note the different time scales for continuous and pulsed irradiation.

Table 1. Temperature-Dependent Rate Constants for the Redox Reaction between 5DSA and 16DSA Embedded in the DMPC Bilayer and $[Ru(bpy)_3]Cl_2$ and $(NH_4)_2S_2O_8$, Using cw- and TR-EPR (Experimental Error ~ 10% for all Rate Constants)

label	T/K	k_{outer} cw-EPR $/10^5$ M^{-1} s^{-1}	k_{inner} cw-EPR $/10^3$ M^{-1} s^{-1}	k_{outer} TR-EPR $/10^5$ M^{-1} s^{-1}
5DSA	275	3.6	4.7	2.8
	283	4.0	6.0	3.2
	304	5.4	6.0	4.8
	310	6.2	15	5.6
16DSA	275	1.8	6.8	1.7
	283	2.0	9.7	2.3
	304	2.4	10	2.7
	310	3.8	33	4.0

as the "flip-flop" motion is known to be extremely slow. Additionally, as proved by the lineshapes of the cw-EPR spectra and by the power saturation EPR experiments on symmetric liposomes, **5DSA** and **16DSA** occupy markedly distinct positions in the bilayer and therefore should give rise to different electron transfer rates.

Following these observations, we solved the kinetic scheme and fitted the different time traces. From the solution, we determined that eqs 1 and 2 of Scheme 3, characterized by k_{outer} and $k_{inner,}$ are the rate-limiting steps. For **5DSA**, k_{outer} increases from 3.6 to 6.2 × 10^5 M^{-1} s^{-1} increasing the temperature from 275 to 310 K (Table 1). The k_{inner} rate constant is two orders of magnitude smaller and increases from 4.7 to 15.0 × 10^3 M^{-1} s^{-1} in the same temperature range. Analogously, for **16DSA**, the rate constants increase from 1.6 to 3.8 × 10^5 M^{-1} s^{-1} and from 6.8 to 33.0 × 10^3 M^{-1} s^{-1}, respectively (Table 1). The observation that the rate constant k_{outer} for **5DSA** is larger than that of **16DSA** by a factor of two (at all temperatures) let us conclude that the nitroxide moiety of **16DSA** is approximately 1 nm more distant from the water/membrane interface (containing the Ru(III) complex) than that of **5DSA** (see also below).[39] Markedly, k_{inner} is bigger for **16DSA** (closer to the outer liposome surface) and smaller for **5DSA**. The rates, which we assign to the oxidation of the nitroxides in the inner leaflet, k_{inner}, are ca. two orders of magnitude lower than k_{outer}.

To verify that the origin of two electron transfer rates have been correctly assessed, we designed an experiment in which the signal decay depends only on the electron transfer rate of the outer leaflet, the fast electron transfer process (k_{outer}). We prepared liposomes that contained $[Ru(bpy)_3]Cl_2$/$(NH_4)_2S_2O_8$ in the external and in the internal aqueous phase (symmetric liposomes), and we employed time-resolved EPR coupled to pulsed-laser irradiation to focus on the microsecond range. Indeed, the decay curves so obtained for the EPR signals of **16DSA** and **5DSA** (Figure 2e−h and Supporting Information Figure S3) display only one component. The corresponding temperature-dependent rate constants are therefore obtained from solution of Scheme S2. They are identical (within the experimental error, Table 1) to those assigned to k_{outer} determined in the steady-state experiment. This clearly underpins the assignment of the two distinctly different time regimes to the ET to the inner and outer leaflets.

In a parallel set of experiments, we used optical spectroscopy to follow the concentration of the oxidant, $[Ru(bpy)_3]^{3+}$, present only in the external aqueous phase, to obtain the absolute rate constant for its formation and to establish its steady-state concentration under our experimental conditions. Upon irradiation of $[Ru(bpy)_3]Cl_2$ in the presence of $(NH_4)_2S_2O_8$, the band at 452 nm of $[Ru(bpy)_3]Cl_2$ decreases

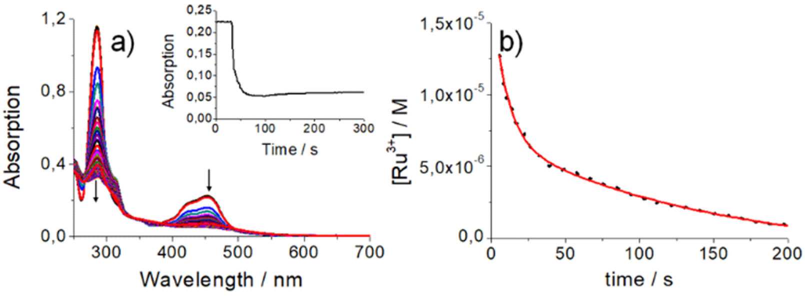

Figure 3. (a) Time-resolved absorption spectrum of $[Ru(bpy)_3]Cl_2$ and $(NH_4)_2S_2O_8$ upon constant irradiation in aqueous solution. The inset shows the absorption change at 452 nm; (b) conversion of $[Ru(bpy)_3]^{3+}$ to $[Ru(bpy)_3]^{2+}$ in the dark in a reaction mixture containing $[Ru(bpy)_3]Cl_2$, $(NH_4)_2S_2O_8$, and DMPC liposomes into which 16DSA had been incorporated (monitored at 452 nm). The fit of the concentration according to Scheme 2 is displayed in red.

within ca. 200 s indicating the oxidation of the Ru(II) species to $[Ru(bpy)_3]^{3+}$ (Figure 3a).[53,70,71]

Finally, to confirm the kinetics of the slow process, we took advantage of UV-vis spectroscopy and followed the reaction with a low time resolution >10 s. A cuvette containing the photoredox system was irradiated for 30 s before each measurement, to convert all the $[Ru(bpy)_3]^{2+}$ to its oxidized form. After injection of the liposomes containing the SNRs, the absorbance at 452 nm was monitored. Indeed, the reappearance of the 452 nm band, after immediate addition of the SNR in the dark, allows us to follow the much slower and rate-determining reduction of $[Ru(bpy)_3]^{3+}$ by SNRs of the inner leaflet, while the one from the outer leaflet is too fast to be detected. Figure 3b displays the concentration of $[Ru(bpy)_3]^{3+}$ as a function of time. The corresponding rate constants at 295 K are 3.5×10^3 M^{-1} s^{-1} for **5DSA** and 8.0×10^3 M^{-1} s^{-1} for **16DSA**; they are close to the values for k_{inner} obtained by cw-EPR.

In order to obtain more information on the kinetics, and in particular on the activation parameters, we have determined the temperature dependence of the k_{inner} and k_{outer} using Eyring theory (see Supporting Information Figure S6); here, the rather small but systematic changes of k_{inner} and k_{outer} (Table 1) afford alike and small free-activation energies, $\Delta G^{\ddagger}$, of ca. 41 kJ/mol for both **5DSA** and **16DSA** (Table 2). Finally, it is necessary to discuss the ET mechanism in the light of our experimental data. It has been shown that tunneling, or superexchange of electrons between sites,[72,73] is a plausible mechanism for ET in phospholipid membranes.[19,20,30,74]

Table 2. Activation Parameters for the Fast ET Calculated from the cw-EPR (cw) and TR-EPR (TR) Data Using the Eyring Equation (Equation S1, See the Supporting Information for More Details)

label	$\Delta H^{\ddagger}$/ (kJ/mol)		$\Delta S^{\ddagger}$ / [J/(mol K)]		$\Delta G^{\ddagger}$/ (kJ/mol)	
	cw	TR	cw	TR	cw	TR
5DSA	8 ± 1	11 ± 1	110 ± 10	110 ± 10	40 ± 4	41 ± 4
16DSA	12 ± 1	11 ± 1	111 ± 9	102 ± 8	42 ± 5	42 ± 5

Our data confirm the low energy barriers that were both predicted and experimentally validated.[1−3]

For tunneling to occur, the donor and acceptor pairs need to interact via an electronic coupling matrix element. Calculation of the electronic coupling elements is possible, on the basis of Marcus theory.[2] A numerical estimation of these elements is provided under the Supporting Information. Naturally, these elements are dependent on the distance and on the medium, following an exponential function. In our case, a distance-decay parameter of 0.5 ± 0.1 nm^{-1} was obtained, a value somewhat similar to others reported for membranes.[74−76] We think that the main reason for the disagreement is the different definition of the distance. We considered geometric distances, whereas in the literature the measurements are conducted electrochemically, thus the technique is likely more sensitive to the apolar part than to the polar one.[75]

Other mechanisms that may be considered for ET in liposomes, such as adiabatic ET, have been ruled out. In fact, adiabatic ET is often characterized by a sensitivity of the ET process to solvent properties, that is, reorganization, whether in an isotropic environment[77] or in a microheterogeneous medium.[78] In our system, the alkyl chains of DMPC can be regarded as a solvent with very slow reorganization capabilities.[78] It is thus likely that the dynamics of the alkyl chains (equivalent to solvent relaxation) would dominate the kinetics of ET and slow down the ET rates, which would be then much lower than in an aqueous solution.[31] However, our data do not display such a decrease in ET rates. Moreover, the temperature dependence does not support an adiabatic mechanism. Finally, involvement of a hopping mechanism appears to be unlikely, since no electroactive component (e.g., an aromatic group) is located between the donor and the acceptor.[79]

■ SUMMARY AND CONCLUSIONS

In the present study it was demonstrated, for the first time, that it is possible to study the kinetics of ET through a lipid membrane bilayer from an electron donor (nitroxide radicals) located within the membrane to a photogenerated Ru(III) in the aqueous solution. Introduction of the spin-label at different positions on the fatty-acid chain permitted construction of a molecular "ruler" for monitoring ET in natural and artificial membrane systems by precise control of the donor/acceptor distance.

We have used this experimental system to determine both the rate constants and activation energies for ET between $[Ru(bpy)_3]^{3+}$ and the nitroxide moieties in **5DSA** and **16DSA** embedded in unilamellar DMPC liposomes. By using both EPR and optical methods, we obtained significant information: (i) We could unequivocally show that the spin labels do not affect the structure of the phospholipid membrane; (ii) we could quantify the penetration depth and the local mobility of the labels **5DSA** and **16DSA**.

https://dx.doi.org/10.1021/acs.langmuir.0c01585
Langmuir XXXX, XXX, XXX−XXX

Our results create a consistent picture for ET through the phospholipid bilayer. Low values of activation energy for ET ($\Delta G^{\ddagger}$ values of 40 ± 4 kJ/mol for **5DSA**, and 42 ± 5 kJ/mol for **16DSA**), as well as the absence of a pronounced effect of the membrane phase transition on the kinetics of ET, provide experimental evidence that ET within the phospholipid bilayer occurs via a tunneling mechanism. We determined a distance dependence of k_{ET} with a β-parameter of 0.5 ± 0.1 nm^{-1}.

The "molecular ruler" methodology that we have developed can be applied not only to phospholipid bilayers, but also to biological membranes, to artificial membranes, and to proteins and protein complexes, thus providing direct experimental information concerning the dynamics of their local environments. It can thus be used, for example, in investigating the involvement of π-electrons and/or water bridges in long-range ET. Since water is always present in membranes (the so called "hydropathy plot"[80]), and EPR signals of nitroxides are sensitive to the polarity of the environment, our approach provides a unique opportunity to studying the roles of water and hydrogen bonds in ET in membranes and proteins (dehydration methods are well known).

EPR spectra of some stable nitroxide radicals (imidazoline and imidazolidine types) are pH-sensitive.[44,51,81] Use of such probes seems extremely promising for simultaneous examination of electron and proton transfer in membrane systems by the EPR approach described here. Their use can provide a unique method for quantitative characterization of proton-coupled ET reactions[82,83] in many important natural and artificial catalytic systems.[84−86]

■ ASSOCIATED CONTENT

Supporting Information

The Supporting Information is available free of charge at https://pubs.acs.org/doi/10.1021/acs.langmuir.0c01585.

Kinetic model, continuous-wave electron paramagnetic resonance (correlation times and attempts of fitting of the signal decays), time-resolved electron paramagnetic resonance (attempts of fittings of the signal decays), small-angle X-ray scattering, dynamic light scattering, Eyring analysis, kinetic parameters of the ET reaction within Marcus theory, and EPR power saturation experiments in liposomes (PDF)

■ AUTHOR INFORMATION

Corresponding Authors

Antonio Barbon − *Dipartimento di Scienze Chimiche, Università degli Studi di Padova, Padova 35131, Italy;* orcid.org/0000-0002-2009-5874; Email: antonio.barbon@unipd.it

Georg Gescheidt − *Institute of Physical and Theoretical Chemistry, Graz University of Technology, Graz 8010, Austria;* orcid.org/0000-0002-6827-4337; Email: g.gescheidt-demner@tugraz.at

Lev Weiner − *Department of Chemical Research Support, Weizmann Institute of Science, Rehovot 76100, Israel;* Email: lev.weiner@weizmann.ac.il

Authors

Max Schmallegger − *Institute of Physical and Theoretical Chemistry, Graz University of Technology, Graz 8010, Austria;* orcid.org/0000-0001-6097-8252

Marco Bortolus − *Dipartimento di Scienze Chimiche, Università degli Studi di Padova, Padova 35131, Italy;* orcid.org/0000-0002-6033-6521

Angela Chemelli − *Institute of Inorganic Chemistry, Graz University of Technology, Graz 8010, Austria*

Itzhak Bilkis − *Faculty of Agricultural, Food and Environmental Sciences, Hebrew University, Rehovot 76100, Israel*

Complete contact information is available at: https://pubs.acs.org/10.1021/acs.langmuir.0c01585

Funding

Progetto di Eccellenza NEXUS, Italian Ministry of University and Research (MIUR). NAWI Graz and COST (EU Commission, action CM1201).

Notes

The authors declare no competing financial interest.

■ ACKNOWLEDGMENTS

A.B. and M.B. acknowledge the support of Progetto Eccellenza NEXUS, and thank Dr. Alfonso Zoleo (University of Padova) for helping with analysis of IR data. We thank NAWI Graz and COST (action CM1201) for supporting this study. M.S. and G.G. are indebted to Dr. Chryssostomos Chatgilialoglu (ISOF Bologna) for his invaluable help in teaching them the basics of liposome preparation and chemistry. The authors thank Prof. Harry B. Gray for helpful discussions and recommendations and Prof. Israel Silman for his constructive suggestions and criticisms during the preparation of the manuscript. The authors wish to acknowledge use of the Somapp Lab, a core facility supported by the Austrian Federal Ministry of Education, Science and Research, the Graz University of Technology, the University of Graz and Anton Paar GmbH.

■ REFERENCES

(1) Gray, H. B.; Winkler, J. R. Electron Transfer in Proteins. *Annu. Rev. Biochem.* **1996**, *65*, 537−561.

(2) Marcus, R. A.; Sutin, N. Electron Transfers in Chemistry and Biology. *Biochim. Biophys. Acta Rev. Bioenerg.* **1985**, *811*, 265−322.

(3) Gray, H. B.; Winkler, J. R. Long-Range Electron Transfer. *Proc. Natl. Acad. Sci. U. S. A.* **2005**, *102*, 3534−3539.

(4) Gray, H. B.; Winkler, J. R. Electron Tunneling through Proteins. *Q. Rev. Biophys.* **2003**, *36*, 341−372.

(5) Chatgilialoglu, C.; Ferreri, C.; Matyjaszewski, K. Radicals and Dormant Species in Biology and Polymer Chemistry. *ChemPlusChem* **2016**, *81*, 11−29.

(6) Giese, B. Long-Distance Charge Transport in DNA: The Hopping Mechanism. *Acc. Chem. Res.* **2000**, *33*, 631−636.

(7) Manetto, A.; Breeger, S.; Chatgilialoglu, C.; Carell, T. Complex Sequence Dependence by Excess-Electron Transfer through DNA with Different Strength Electron Acceptors. *Angew. Chem., Int. Ed. Engl.* **2005**, *45*, 318−321.

(8) Astruc, D. Electron-Transfer Processes in Dendrimers and Their Implication in Biology, Catalysis, Sensing and Nanotechnology. *Nat. Chem.* **2012**, *4*, 255−267.

(9) Gust, D.; Moore, T. A.; Moore, A. L. Mimicking Photosynthetic Solar Energy Transduction. *Acc. Chem. Res.* **2001**, *34*, 40−48.

(10) Fukuzumi, S.; Ohkubo, K.; Suenobu, T. Long-Lived Charge Separation and Applications in Artificial Photosynthesis. *Acc. Chem. Res.* **2014**, *47*, 1455−1464.

(11) Grätzel, M. Light Energy Harvesting and Photoinduced Electron Transfer in Organized Molecular Assemblies. In *Heterogeneous Photochemical Electron Transfer*; CRC Press, 1989; pp. 43−86.

(12) Robinson, J. N.; Cole-Hamilton, D. J. Electron Transfer across Vesicle Bilayers. *Chem. Soc. Rev.* **1991**, *20*, 49−94.

(13) de Rege, P.; Williams, S.; Therien, M. Direct Evaluation of Electronic Coupling Mediated by Hydrogen Bonds: Implications for Biological Electron Transfer. *Science* **1995**, *269*, 1409−1413.
(14) Nicholls, P.; West, J.; Bangham, A. D. Chlorophyll b Containing Liposomes: Effect of Thermal Transitions on Catalytic and Spectral Properties. *Biochim. Biophys. Acta Biomembr.* **1974**, *363*, 190−201.
(15) Woodle, M.; Zhang, J. W.; Mauzerall, D. Kinetics of Charge Transfer at the Lipid Bilayer-Water Interface on the Nanosecond Time Scale. *Biophys. J.* **1987**, *52*, 577−586.
(16) Zamaraev, K. I.; Lymar, S. V.; Khramov, M. I.; Parmon, V. N. Vectorial Phototransfer of Electrons across Lipid Membranes. *Pure Appl. Chem.* **1988**, *60*, 1039−1046.
(17) Ford, W. E.; Tollin, G. Chlorophyll Photosensitized Electron Transfer in Phospholipid Vesicle Bilayers: Inside Vs Outside Asymmetry. *Photochem. Photobiol.* **1982**, *36*, 647−655.
(18) Tomkiewicz, M.; Corker, G. A. Diffusion Kinetics in Phospholipid Vesicles. *Chem. Phys. Lett.* **1976**, *37*, 537−542.
(19) Ford, W. E.; Tollin, G. Direct Observation of Electron Transfer Across a Lipid Bilayer: Pulsed Laser Photolysis of an Asymmetric Vesicle System Containing Chlorophyll, Methyl Viologen and Edta. *Photochem. Photobiol.* **1982**, *35*, 809−819.
(20) Laane, C.; Ford, W. E.; Otvos, J. W.; Calvin, M. Photosensitized Electron Transport across Lipid Vesicle Walls: Enhancement of Quantum Yield by Ionophores and Transmembrane Potentials. *Proc. Natl. Acad. Sci. U. S. A.* **1981**, *78*, 2017−2020.
(21) Piotrowiak, P. Photoinduced Electron Transfer in Molecular Systems: Recent Developments. *Chem. Soc. Rev.* **1999**, *28*, 143−150.
(22) Bhosale, S.; Sisson, A. L.; Talukdar, P.; Fürstenberg, A.; Banerji, N.; Vauthey, E.; Bollot, G.; Mareda, J.; Röger, C.; Würthner, F.; Sakai, N.; Matile, S. Photoproduction of Proton Gradients with π-Stacked Fluorophore Scaffolds in Lipid Bilayers. *Science* **2006**, *313*, 84−86.
(23) El Maghraby, G. M.; Barry, B. W.; Williams, A. C. Liposomes and Skin: From Drug Delivery to Model Membranes. *Eur. J. Pharm. Sci.* **2008**, *34*, 203−222.
(24) Sessa, G.; Weissmann, G. Phospholipid Spherules (Liposomes) as a Model for Biological Membranes. *J. Lipid Res.* **1968**, *9*, 310−318.
(25) Ferreri, C.; Chatgilialoglu, C. Free Radicals and Lipids. In *Membrane Lipidomics for Personalized Health*; 2015; *21*, pp. 300−302.
(26) Dalzini, A.; Bergamini, C.; Biondi, B.; De Zotti, M.; Panighel, G.; Fato, R.; Peggion, C.; Bortolus, M.; Maniero, A. L. The Rational Search for Selective Anticancer Derivatives of the Peptide Trichogin GA IV: A Multi-Technique Biophysical Approach. *Sci. Rep.* **2016**, *6*, 24000.
(27) Mobbili, G.; Crucianelli, E.; Barbon, A.; Marcaccio, M.; Pisani, M.; Dalzini, A.; Ussano, E.; Bortolus, M.; Stipa, P.; Astolfi, P. Liponitroxides: EPR Study and Their Efficacy as Antioxidants in Lipid Membranes. *RSC Adv.* **2015**, *5*, 98955−98966.
(28) Hurley, J. K.; Castelli, F.; Tollin, G. Chlorophyll Photochemistry In Condensed Media—II. Triplet State Quenching And Electron Transfer To Quinone In Liposomes. *Photochem. Photobiol.* **1980**, *32*, 79−86.
(29) Limburg, B.; Bouwman, E.; Bonnet, S. Catalytic Photoinduced Electron Transport across a Lipid Bilayer Mediated by a Membrane-Soluble Electron Relay. *Chem. Commun.* **2015**, *51*, 17128−17131.
(30) Ford, W. E.; Otvos, J. W.; Calvin, M. Photosensitized Electron Transport across Lipid Vesicle Walls: Quantum Yield Dependence on Sensitizer Concentration. *Proc. Natl. Acad. Sci. U. S. A.* **1979**, *76*, 3590−3593.
(31) Eliash, T.; Barbon, A.; Brustolon, M.; Sheves, M.; Bilkis, I.; Weiner, L. Nitroxyl Radicals for Studying Electron Transfer. *Angew. Chem., Int. Ed. Engl.* **2013**, *52*, 8689−8692.
(32) Zerbi, G.; Barbon, A.; Bengalli, R.; Lucotti, A.; Catelani, T.; Tampieri, F.; Gualtieri, M.; D'Arienzo, M.; Morazzoni, F.; Camatini, M. Graphite Particles Induce ROS Formation in Cell Free Systems and Human Cells. *Nanoscale* **2017**, *9*, 13640−13650.
(33) Alaouie, A. M.; Smirnov, A. I. Ultra-Stable Temperature Control in EPR Experiments: Thermodynamics of Gel-to-Liquid Phase Transition in Spin-Labeled Phospholipid Bilayers and Bilayer Perturbations by Spin Labels. *J. Magn. Reson.* **2006**, *182*, 229−238.
(34) Perissi, I.; Ristori, S.; Rossi, S.; Dei, L.; Martini, G. Electron Spin Resonance and Differential Scanning Calorimetry as Combined Tools for the Study of Liposomes in the Presence of Long Chain Nitroxides. *J. Phys. Chem. B* **2002**, *106*, 10468−10473.
(35) Pentak, D. Alternative Methods of Determining Phase Transition Temperatures of Phospholipids That Constitute Liposomes on the Example of DPPC and DMPC. *Thermochim. Acta* **2014**, *584*, 36−44.
(36) Stimson, L.; Dong, L.; Karttunen, M.; Wisniewska, A.; Dutka, M.; Róg, T. Stearic Acid Spin Labels in Lipid Bilayers: Insight through Atomistic Simulations. *J. Phys. Chem. B* **2007**, *111*, 12447−12453.
(37) Hubbell, W. L.; McConnell, H. M. Motion Of Steroid Spin Labels In Membranes. *Proc. Natl. Acad. Sci. U. S. A.* **1969**, *63*, 16−22.
(38) Hubbell, W. L.; McConnell, H. M. Molecular Motion in Spin-Labeled Phospholipids and Membranes. *J. Am. Chem. Soc.* **1971**, *93*, 314−326.
(39) Vartorelli, M. R.; Garay, A. S.; Rodrigues, D. E. Spin-Labeled Stearic Acid Behavior and Perturbations on the Structure of a Gel-Phase-Lipid Bilayer in Water: 5-, 12- And 16-SASL. *J. Phys. Chem. B* **2008**, *112*, 16830−16842.
(40) Nagle, J. F. Theory of the Main Lipid Bilayer Phase Transition. *Annu. Rev. Phys. Chem.* **1980**, *31*, 157−196.
(41) Fendler, J. H. Atomic and Molecular Clusters in Membrane Mimetic Chemistry. *Chem. Rev.* **1987**, *87*, 877−899.
(42) Wu, E.-S.; Jacobson, K.; Papahadjopoulos, D. Lateral Diffusion in Phospholipid Multibilayers Measured by Fluorescence Recovery after Photobleaching. *Biochemistry* **1977**, *16*, 3936−3941.
(43) Tabushi, I.; Hamachi, I.; Kobuke, Y. Control of Electron Transport by Thermally Induced Phase Transition of Liposomal Membrane. *Tetrahedron Lett.* **1987**, *28*, 5899−5902.
(44) Weiner, L. M. Stable Nitroxyl Radicals as pH, Thiol and Electron Transfer Probes. *Appl. Magn. Reson.* **2007**, *31*, 357−373.
(45) Lewandowska-Andralojc, A.; Polyansky, D. E. Mechanism of the Quenching of the Tris(Bipyridine)Ruthenium(II) Emission by Persulfate: Implications for Photoinduced Oxidation Reactions. *J. Phys. Chem. A* **2013**, *117*, 10311−10319.
(46) Bolletta, F.; Maestri, M.; Moggi, L.; Balzani, V. Dynamic and Static Quenching of the Tris(2,2′-Dipyridyl)Ruthenium(II) Phosphorescence by Anionic Coordination Compounds in Various Solvents. *J. Phys. Chem.* **1974**, *78*, 1374−1377.
(47) Henbest, K.; Douglas, P.; Garley, M. S.; Mills, A. Persulphate Quenching of the Excited State of Ruthenium(II) Tris-Bipyridyl Dication: Thermal Reactions. *J. Photochem. Photobiol. A Chem.* **1994**, *80*, 299−305.
(48) Horváth, A.; Bakó, Z.; Papp, S.; Keszei, C. S. Oxidative Quenching of Excited $Ru(Bpy)_3^{2+}$ with $S_2O_8^{2-}$ at Various pH and External Magnetic Field Values. *J. Photochem. Photobiol. A Chem.* **1990**, *52*, 271−280.
(49) Kaledin, A. L.; Huang, Z.; Yin, Q.; Dunphy, E. L.; Constable, E. C.; Housecroft, C. E.; Geletii, Y. V.; Lian, T.; Hill, C. L.; Musaev, D. G. Insights into Photoinduced Electron Transfer between $[Ru(Mptpy)_2]^{4+}$ (Mptpy = 4′(4-Methylpyridinio)-2,2′:6′,2″-Terpyridine) and $[S_2O_8]^{2-}$: Computational and Experimental Studies. *J. Phys. Chem. A* **2010**, *114*, 6284−6297.
(50) White, H. S.; Becker, W. G.; Bard, A. J. Photochemistry of the Tris(2,2′-Bipyridine)Ruthenium(II)-Peroxydisulfate System in Aqueous and Mixed Acetonitrile-Water Solutions. Evidence for a Long-Lived Photoexcited Ion Pair. *J. Phys. Chem.* **1984**, *88*, 1840−1846.
(51) Barbon, A.; Bortolus, M.; Isse, A. A.; Reznikov, V. A.; Weiner, L. Electron Transfer in PH-Sensitive Nitroxide Radicals. *Chem. Phys. Lett.* **2016**, *665*, 137−140.
(52) Ford, W. E.; Rodgers, M. A. J. Kinetics of Nitroxyl Radical Oxidation by $Ru(Bpy)_3^{3+}$ Following Photosensitization of Antimony-Doped Tin Dioxide Colloidal Particles. *J. Phys. Chem. B* **1997**, *101*, 930−936.

https://dx.doi.org/10.1021/acs.langmuir.0c01585
Langmuir XXXX, XXX, XXX−XXX

(53) Morris, N. D.; Suzuki, M.; Mallouk, T. E. Kinetics of Electron Transfer and Oxygen Evolution in the Reaction of $Ru(Bpy)_3^{3+}$ with Colloidal Iridium Oxide. *J. Phys. Chem. A* **2004**, *108*, 9115−9119.
(54) Dua, J. S.; Rana, A. C.; Bhandari, A. K. Liposome: Methods of Preparation and Application. *Int. J. Pharm. Stud. Res.* **2012**, *3*, 14−20.
(55) Orthaber, D.; Bergmann, A.; Glatter, O. SAXS Experiments on Absolute Scale with Kratky Systems Using Water as a Secondary Standard. *J. Appl. Crystallogr.* **2000**, *33*, 218−225.
(56) Glatter, O. A New Method for the Evaluation of Small-Angle Scattering Data. *J. Appl. Crystallogr.* **1977**, *10*, 415−421.
(57) Glatter, O. The Interpretation of Real-Space Information from Small-Angle Scattering Experiments. *J. Appl. Crystallogr.* **1979**, *12*, 166−175.
(58) Frühwirth, T.; Fritz, G.; Freiberger, N.; Glatter, O. Structure and Order in Lamellar Phases Determined by Small-Angle Scattering. *J. Appl. Crystallogr.* **2004**, *37*, 703−710.
(59) Schnablegger, H.; Glatter, O. Optical Sizing of Small Colloidal Particles: An Optimized Regularization Technique. *Appl. Opt.* **1991**, *30*, 4889−4896.
(60) Etienne, E.; Le Breton, N.; Martinho, M.; Mileo, E.; Belle, V. SimLabel: A Graphical User Interface to Simulate Continuous Wave EPR Spectra from Site-Directed Spin Labeling Experiments. *Magn. Reson. Chem.* **2017**, *55*, 714−719.
(61) Altenbach, C.; Greenhalgh, D. A.; Khorana, H. G.; Hubbell, W. L. A Collision Gradient Method to Determine the Immersion Depth of Nitroxides in Lipid Bilayers: Application to Spin-Labeled Mutants of Bacteriorhodopsin. *Proc. Natl. Acad. Sci. U. S. A.* **1994**, *91*, 1667−1671.
(62) Laudadio, E.; Galeazzi, R.; Mobbili, G.; Minnelli, C.; Barbon, A.; Bortolus, M.; Stipa, P. Depth Distribution of Spin-Labeled Liponitroxides within Lipid Bilayers: A Combined EPR and Molecular Dynamics Approach. *ACS Omega* **2019**, *4*, 5029−5037.
(63) Hoops, S.; Gauges, R.; Lee, C.; Pahle, J.; Simus, N.; Singhal, M.; Xu, L.; Mendes, P.; Kummer, U. COPASI - A COmplex PAthway SImulator. *Bioinformatics* **2006**, *22*, 3067−3074.
(64) Subczynski, W. K.; Raguz, M.; Widomska, J. Studying Lipid Organization in Biological Membranes Using Liposomes and EPR Spin Labeling. *Methods Mol. Biol.* **2010**, *606*, 247−269.
(65) Brustolon, M.; Giamello, E. *Electron Paramagnetic Resonance: A Practitioner's Toolkit*; Wiley, 2009.
(66) Marsh, D. Electron Spin Resonance: Spin Labels. In *Membrane Spectroscopy*; Grell, E., Ed.; Springer, 1981; pp. 51−142.
(67) Conte, E.; Maria, F.; Khandelia, H.; Jeschke, G.; Bordignon, E. Lipid Peroxidation and Water Penetration in Lipid Bilayers: A W-Band EPR Study. *Biochim. Biophys. Acta Biomembr.* **2013**, *1828*, 510−517.
(68) Bortolus, M.; Dalzini, A.; Formaggio, F.; Toniolo, C.; Gobbo, M.; Maniero, A. L. An EPR Study of Ampullosporin A, a Medium-Length Peptaibiotic, in Bicelles and Vesicles. *Phys. Chem. Chem. Phys.* **2016**, *18*, 749−760.
(69) Dzikovski, B.; Livshits, V.; Freed, J. Interaction of Spin-Labeled Lipid Membranes with Transition Metal Ions. *J. Phys. Chem. B* **2015**, *119*, 13330−13346.
(70) Juris, A.; Balzani, V.; Barigelletti, F.; Campagna, S.; Belser, P.; von Zelewsky, A. Ru(II) Polypyridine Complexes: Photophysics, Photochemistry, Eletrochemistry, and Chemiluminescence. *Coord. Chem. Rev.* **1988**, *84*, 85−277.
(71) Kalyanasundaram, K.; Graetzel, M.; Nazeeruddin, M. K. Excited-State Interactions in Ligand-Bridged Chromophore-Quencher Complexes Containing Rhodium(III) and Ruthenium(II) Polypyridyl Units. *J. Phys. Chem.* **1992**, *96*, 5865−5872.
(72) Ponce, A.; Gray, H. B.; Winkler, J. R. Electron Tunneling through Water: Oxidative Quenching of Electronically Excited $Ru(Tpy)_2^{2+}$ (Tpy = 2,2′:6,2″-Terpyridine) by Ferric Ions in Aqueous Glasses at 77 K. *J. Am. Chem. Soc.* **2000**, *122*, 8187−8191.
(73) Wenger, O. S.; Leigh, B. S.; Villahermosa, R. M.; Gray, H. B.; Winkler, J. R. Electron Tunneling through Organic Molecules in Frozen Glasses. *Science* **2005**, *307*, 99−102.
(74) Hurst, J. K.; Thompson, D. H. P. Mechanisms of Oxidation—Reduction across Vesicle Bilayer Membranes: An Overview. *J. Memb. Sci.* **1986**, *28*, 3−29.
(75) Campos, R.; Kataky, R. Electron Transport in Supported and Tethered Lipid Bilayers Modified with Bioelectroactive Molecules. *J. Phys. Chem. B* **2012**, *116*, 3909−3917.
(76) Sarangi, N. K.; Patnaik, A. L-Tryptophan-Induced Electron Transport across Supported Lipid Bilayers: An Alkyl-Chain Tilt-Angle, and Bilayer-Symmetry Dependence. *ChemPhysChem* **2012**, *13*, 4258−4270.
(77) Polimeno, A.; Barbon, A.; Nordio, P. L.; Rettig, W. Stochastic Model for Solvent-Assisted Intramolecular Charge-Transfer. *J. Phys. Chem.* **1994**, *98*, 12158−12168.
(78) Pansu, R. B.; Yoshihara, K. Diffusion of Excited Bianthryl in Microheterogeneous Media. *J. Phys. Chem.* **1991**, *95*, 10123−10133.
(79) Ricks, A. B.; Brown, K. E.; Wenninger, M.; Karlen, S. D.; Berlin, Y. A.; Co, D. T.; Wasielewski, M. R. Exponential Distance Dependence of Photoinitiated Stepwise Electron Transfer in Donor-Bridge-Acceptor Molecules: Implications for Wirelike Behavior. *J. Am. Chem. Soc.* **2012**, *134*, 4581−4588.
(80) Degli Esposti, M.; Crimi, M.; Venturoli, G. A Critical Evaluation of the Hydropathy Profile of Membrane Proteins. *Eur. J. Biochem.* **1990**, *190*, 207−219.
(81) Zottler, E.; Gescheidt, G. Nitroxides: Versatile Reporters and Reactants. *J. Chem. Res.* **2011**, *35*, 257−267.
(82) Cukier, R. I.; Nocera, D. G. Proton-Coupled Electron Transfer. *Annu. Rev. Phys. Chem.* **1998**, *49*, 337−369.
(83) Weinberg, D. R.; Gagliardi, C. J.; Hull, J. F.; Murphy, C. F.; Kent, C. A.; Westlake, B. C.; Paul, A.; Ess, D. H.; McCafferty, D. G.; Meyer, T. J. Proton-Coupled Electron Transfer. *Chem. Rev.* **2012**, *112*, 4016−4093.
(84) Hammes-Schiffer, S.; Soudackov, A. V. Proton-Coupled Electron Transfer in Solution, Proteins, and Electrochemistry. *J. Phys. Chem. B* **2008**, *112*, 14108−14123.
(85) Reece, S. Y.; Nocera, D. G. Proton-Coupled Electron Transfer in Biology: Results from Synergistic Studies in Natural and Model Systems. *Annu. Rev. Biochem.* **2009**, *78*, 673−699.
(86) Gentry, E. C.; Knowles, R. R. Synthetic Applications of Proton-Coupled Electron Transfer. *Acc. Chem. Res.* **2016**, *49*, 1546−1556.

https://dx.doi.org/10.1021/acs.langmuir.0c01585
Langmuir XXXX, XXX, XXX−XXX